Available online at www.sciencedirect.com
SCIENCE DIRECT
Geochimica et Cosmochimica Acta 70 (2006) 3299–3312
Geochimica
www.elsevier.com/locate/gca

Quantitative antimony speciation in shooting-range soils by EXAFS spectroscopy

Andreas C. Scheinost [a,*], Andre Rossberg [a], Delphine Vantelon [b,1], Irene Xifra [b], Ruben Kretzschmar [b], Ann-Kathrin Leuz [c], Harald Funke [a], C. Annette Johnson [c]

[a] Institute of Radiochemistry, FZR, 01314 Dresden, Germany
[b] Institute of Terrestrial Ecology, ETHZ, 8092 Zurich, Switzerland
[c] Swiss Federal Institute of Environmental Science and Technology (EAWAG), 8600 Dübendorf, Switzerland

Received 14 March 2005; accepted in revised form 20 March 2006

Abstract

The Sb speciation in soil samples from Swiss shooting ranges was determined using Sb K-edge X-ray absorption spectroscopy (XAS) and advanced statistical data analysis methods (iterative transformation factor analysis, ITFA). The XAS analysis was supported by a spectral data set of 13 Sb minerals and 4 sorption complexes. In spite of a high variability in geology, soil pH (3.1–7.5), Sb concentrations (1000–17,000 mg/kg) and shooting-range history, only two Sb species were identified. In the first species, Sb is surrounded solely by other Sb atoms at radial distances of 2.90, 3.35, 4.30 and 4.51 Å, indicative of metallic Sb(0). While part of this Sb(0) may be hosted by unweathered bullet fragments consisting of PbSb alloy, Pb L_{III}-edge XAS of the soil with the highest fraction (0.75) of Sb(0) showed no metallic Pb, but only Pb^{2+} bound to soil organic matter. This suggests a preferential oxidation of Pb in the alloy, driven by the higher standard reduction potential of Sb. In the second species, Sb is coordinated to 6 O-atoms at a distance of 1.98 Å, indicative of Sb(V). This oxidation state is further supported by an edge energy of 30,496–30,497 eV for the soil samples with <10% Sb(0). Iron atoms at radial distances of 3.10 and 3.56 Å from Sb atoms are in line with edge-sharing and bidentate corner-sharing linkages between $Sb(O,OH)_6$ and $Fe(O,OH)_6$ octahedra. While similar structural units exist in tripuhyite, the absence of Sb neighbors contradicts formation of this Fe antimonate. Hence the second species most likely consists of inner-sphere sorption complexes on Fe oxides, with edge and corner-sharing configuration occurring simultaneously. This pentavalent Sb species was present in all samples, suggesting that it is the prevailing species after weathering of metallic Sb(0) in oxic soils. No indication of Sb(III) was found.

1. Introduction

Antimony is the 9th most exploited metal worldwide with 140,000 mg being mined each year. It is used in non-metal products as antimony trioxide (Sb_2O_3), primarily in flame retardants, but also as a catalyst in plastics, for the fining of glassware, and as pigment in paints and lacquers. Metallic Sb is used to harden Pb alloys for the manufacture of products such as acid–lead batteries, bearings and ammunition (Adriano, 1986; Krachler et al., 2001). Global emissions of Sb to the atmosphere from both natural and anthropogenic sources are estimated to be 6000 mg per year (Filella et al., 2002). Important sources of uncontrolled release of Sb into the environment are road traffic (dust from break linings and tires), older battery producing plants and shooting ranges. Antimony concentrations up to several thousand milligrams per kilogram have been reported for soils influenced by mining activities (Filella et al., 2002). In the soils of shooting ranges, Sb concentrations of up to 100 g kg^{-1} have been found, which is 6 orders of magnitude above the natural background of 0.1 mg kg^{-1} (Fahrenhorst and Renger, 1990; Basunia and

* Corresponding author. Address: The Rossendorf Beamline at ESRF, BP 220, F-38043 Grenoble Cedex, France. Fax: +33 476 88 25 05.
E-mail address: scheinost@esrf.fr (A.C. Scheinost).
[1] Present address: Synchrotron SOLEIL, 91192 Gif sur Yvette cedex, France.

0016-7037/$ - see front matter © 2006 Elsevier Inc. All rights reserved.
doi:10.1016/j.gca.2006.03.020

Landsberger, 2001; Knechtenhofer et al., 2003; Johnson et al., 2005). The Pb cores of Swiss army bullets contain 2–5% of Sb. Since approximately 500 mg of these bullets are deposited on shooting ranges per year in Switzerland alone, 10–25 mg of Sb are emitted, representing a major emission path.

The toxicity of Sb is thought to be similar to that of As. It is therefore to be expected that Sb does not have a strong ecotoxicological effect, but may be mutagenic. Trivalent compounds have a ten times higher acute toxicity than pentavalent species (Krachler et al., 2001). Even more critical due to its radiotoxicity is the gamma-emitting radionuclide ^{125}Sb. This radionuclide, which is a fission product of ^{253}U with a half-life of 2.8 years, is found at nuclear waste disposal sites (Anonymous, 1998). In spite of the common usage and probable substantial toxicity, little is known on the speciation and geochemical fate of Sb in soils and sediments (Krupka and Serne, 2002). Superficially deposited Sb seems to be retained in the topsoils, since concentrations rapidly decline with soil depth (Ainsworth et al., 1990; Fahrenhorst and Renger, 1990; Knechtenhofer, 2002). However, Johnson et al. (2005) found evidence that Sb(V) may be quite mobile in contaminated soils. The oxidation state has a critical influence on the mobility of Sb in soils. Under oxic conditions, the pentavalent Sb species $Sb(OH)_6^-$ should prevail in soil solution at pH > 2.5. This anionic hydrolysis species is adsorbed by Fe oxides at low pH, but should be mobile above their point of zero charge, i.e., at neutral and basic pH values (Crecelius et al., 1975; Legoux et al., 1992; Blay, 2000). Under reducing conditions, the trivalent neutral complex, $Sb(OH)_3^0$, is expected to be the most stable species, which sorbs to Fe oxides over a wide pH range, hence is expected to be rather immobile even in neutral soils (Crecelius et al., 1975; Blay, 2000). Making predictions of Sb mobility even more complicated, significant fractions of Sb(V) have been found in anoxic waters, and Sb(III) has been found in oxic waters (Filella et al., 2002), in line with slow reduction and oxidation kinetics (Leuz and Johnson, 2005).

Antimony speciation attempts of bulk soil and sediment samples have been made early on by selective sequential extraction, suggesting association of Sb with Fe oxides (Crecelius et al., 1975; Blay, 2000); however, this method is prone to a range of pitfalls (Kim and Fergusson, 1991; Bunzl et al., 1999; Calmano et al., 2001). In situ analysis of species by EXAFS spectroscopy has proven to be a powerful tool for metal speciation in soils (Manceau et al., 1996), especially if supplemented by synchrotron microbeam techniques such as μ-XRF, μ-XAS and μ-XRD (Manceau et al., 2000; Roberts et al., 2002), by advanced statistical analysis tools (Wasserman et al., 1999; Rossberg et al., 2003; Scheinost et al., 2005), or by chemical extractions (Scheinost et al., 2002). XAS has only rarely been applied to Sb speciation, with a prime focus on the determination of Sb complexation with chloride and sulfide in aqueous solutions (Oelkers et al., 1998; Mosselmans et al., 2000; Sherman et al., 2000). Therefore, this is the first attempt to apply XAS spectroscopy to solve Sb speciation in soil samples. A spectral data base of Sb mineral phases and sorption complexes was established to interpret the soil data. Shooting-range soils were selected because the Sb concentrations are sufficiently high for XAS analysis, and because shooting activities are an important emitter of Sb into the environment.

2. Materials and methods

Nine soils samples were collected at six shooting ranges in Switzerland, representing a wide range of geochemical conditions including pH, organic and inorganic carbon content and mineralogy, and representing a range of Sb pollution levels (Table 1). The predominant ammunition used at these sites are two calibers of rifle bullets, 6.5 mm (GP11) and 7.5 mm (GW Pat 90), consisting of a metallic core of Pb hardened with 2–5% Sb, encased in a cupronickel-clad steel jacket. Soil samples were collected at the stop butts (Quartino, Davos, Goldau, and Oberuzwil) and behind the stop butts (Losone and Zuchwil) in various depths as indicated, air dried and sieved (<2 mm or <0.5 mm). The elemental composition was determined by energy-dispersive X-ray fluorescence spectrometry (Spectro X-LAB 2000).

The Sb mineral samples sénarmontite, valentinite, stibiconite, and cervantite were provided by M.O. Figueiredo, Crystal and Mineral Centre, Lisboa, Portugal. Cubic Sb_2O_3 and Sb_2O_5 were reagent grade chemicals from Fluka and Aldrich, respectively. Roméite, bindheimite, tripuhyite, brizziite, Al antimonate, Cu antimonate and K antimonate were precipitated from aqueous solutions at room temperature and then aged at 70–80 °C for 2 weeks. The phase identity of all solids was confirmed by powder XRD. Sorption samples were prepared by reacting 9 mg L^{-1} Sb and 3 g L^{-1} goethite. Sb^{3+} sorbed goethite was prepared from a Sb(III) standard solution (1002 mg L^{-1} Sb_2O_3, CertiPUR) in 2 M HCl, and Sb^{5+} sorbed goethite was prepared from $KSb(OH)_6$. The pH was adjusted to 3.2. The samples were shaken in the dark for 4 days, then filtered with Whatman filter <0.45 μm and freeze-dried. For the Sb^{3+} sorbed humic acid, 20 mL of the Sb(III) standard solution was titrated with NaOH to pH 5, and then 5 g of humic acid (Aldrich) was added.

Antimony K-edge XAS spectra were collected at the Rossendorf Beamline (BM20) at the ESRF. Both the X-ray absorption near-edge spectroscopy (XANES) region around the absorption edge, and the extended X-ray absorption fine structure (EXAFS) region above the absorption edge were recorded. The Si(1 1 1) monochromator energy was calibrated relative to the Sb K-edge of metallic antimony (30,491 eV). Soil samples were measured in fluorescence mode using a 4-element Ge detector. Reference samples were diluted in Teflon powder, pressed to pellets and measured in transmission mode. Sample cooling to 20 K using a He cryostat greatly improved spectral quality due to reduction of the thermal contributions to the

Table 1
Soil sample properties

Sample	Depth (cm)	pH	$CaCO_3$ (g/kg)	Corg (g/kg)	Sb (mg/kg)	Pb (mg/kg)	Cu (mg/kg)
Losone N4	16	3.6	0	150	1300	21,300	43
Losone J-1	1	3.2	0	330	4000	80,900	189
Quartino[a]	0–5	9.4	73	72	17,500	>500,000	4450
Davos[a]	0–5	7.8	133	6	1900	35,000	920
Oberuzwil 0–5	0–5	6.9	0	300	8000	171,000	2720
Oberuzwil 5–15	5–15	7.1	13	220	3400	76,000	2080
Oberuzwil BC	25–45	7.1	53	220	8600	175,000	5100
Goldau[a]	0–5	8.2	335	29	6000	111,000	3050
Zuchwil	0–5	5.8	0	50	1600	21,000	2750

[a] <0.5 mm fraction.

Debye–Waller factors, and was routinely applied. Each single scan of a sample was corrected for energy using a simultaneously monitored Sb(0) foil, and was corrected for the dead time of the fluorescence detector with SixPack (http://www.stanford.edu/~swebb) before averaging the scans. Quantitative speciation was performed by applying iterative transformation factor analysis (ITFA) to the set of k^3-weighted chi spectra (Rossberg et al., 2003; Scheinost et al., 2005). To determine the short-range structure of extracted species, EXAFS shell fitting was performed using FEFF 7 and WinXAS (Ankudinov and Rehr, 1997; Ressler, 1998). Based on the fits of reference minerals, the error of the first shell coordination numbers is better than ±25%, and the error of distances is ±0.01 Å. The monitored XANES region has a relatively poor energy resolution due to the core hole lifetime of Sb (3 eV) and due to the resolution of the Si(1 1 1) monochromator crystal (4 eV) at 30.4 keV, hence only one main inflexion point was determined at the absorption edge by the knot of the second derivative. Lead L-III edge EXAFS spectra of soil samples and of reference compounds were collected on beamline X-11A (National Synchrotron Light Source, Upton, New York) and on the Rossendorf Beamline (ESRF), using a Lytle-type detector for fluorescence detection, and sample cooling with liquid nitrogen.

3. Results and discussion

3.1. Local structure of Sb references

Antimony has the electron configuration $[Kr]4d^{10}5s^25p^3$, which explains the stability of oxidation states Sb(III) and Sb(V). The lone electron pair $5s^2$ of Sb(III) is strongly localized; hence Sb(III) coordination is asymmetric, similar to Pb(II).Three bonds point away from the lone electron pair, forming a trigonal pyramidal coordination (Fig. 1). This rule seems to be broken only by nadorite, where Sb^{3+} binds to 4 oxygen atoms (Giuseppetti and Tadini, 1973). In contrast, Sb(V) is octahedrally coordinated to 6 oxygen atoms, in line with the symmetric $4d^{10}$ electron configuration (Fig. 1). Hence Sb(III) and Sb(V) species are easily discriminated by their O-coordination numbers.

Since little work exists on how chemical Sb species can be identified based on their local structure, we compiled

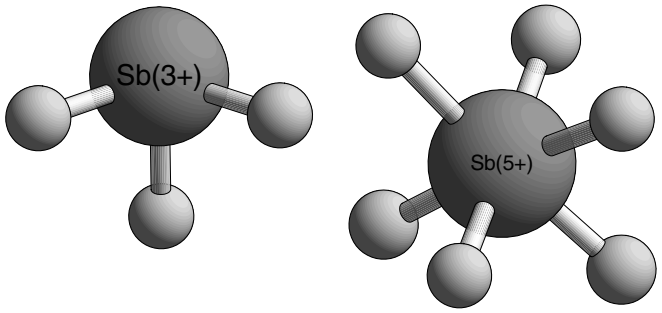

Fig. 1. Coordination of Sb(III) and Sb(V) in oxide minerals. Oxygen atoms are indicated by the smaller balls. For both oxidation states, Sb—O distances largely overlap (1.92–2.04 Å for Sb(III) and 1.98–2.10 Å for Sb(V)).

structure data of 28 Sb compounds, which may occur in shooting-range soils based on their oxidation state (0, III, V) and elemental composition (Fig. 2) (Anonymous, 2004). The pentavalent and mixed oxidation state compounds (Fig. 2, top) show a particularly wide variety of nearest and next-nearest metal distances, ranging from 3.05 Å in spinel and rutile-like structures, up to 4.9 Å in the insular structures of brandholzite and bottinoite. In general, an unequivocal identification of specific Sb compounds seems to be possible only, if the local structure can be determined for radial distances up to 5 Å, a condition that commonly requires dampening of thermal oscillations by cryostatic temperature during data acquisition. Furthermore, we measured XAS spectra of 18 reference phases in order to establish a spectral data base and to check the reliability of the EXAFS fit procedure.

3.1.1. Simple oxides

Fig. 3 and Table 2 give the XANES and EXAFS spectra and fit results of simple trivalent, pentavalent and mixed Sb oxides. The XANES spectra of the trivalent oxides (Sb_2O_3 Fluka, sénarmontite and valentinite) have a lower edge energy (30,493 eV) and a less pronounced white line in comparison to the pentavalent oxide (30,497 eV). The corresponding characteristics of the mixed oxides stibiconite and cervantite are closer to those of the pentavalent oxide. The three trivalent oxides are clearly separated from the higher oxides by their small O-peaks in the EXAFS Fourier transforms (at

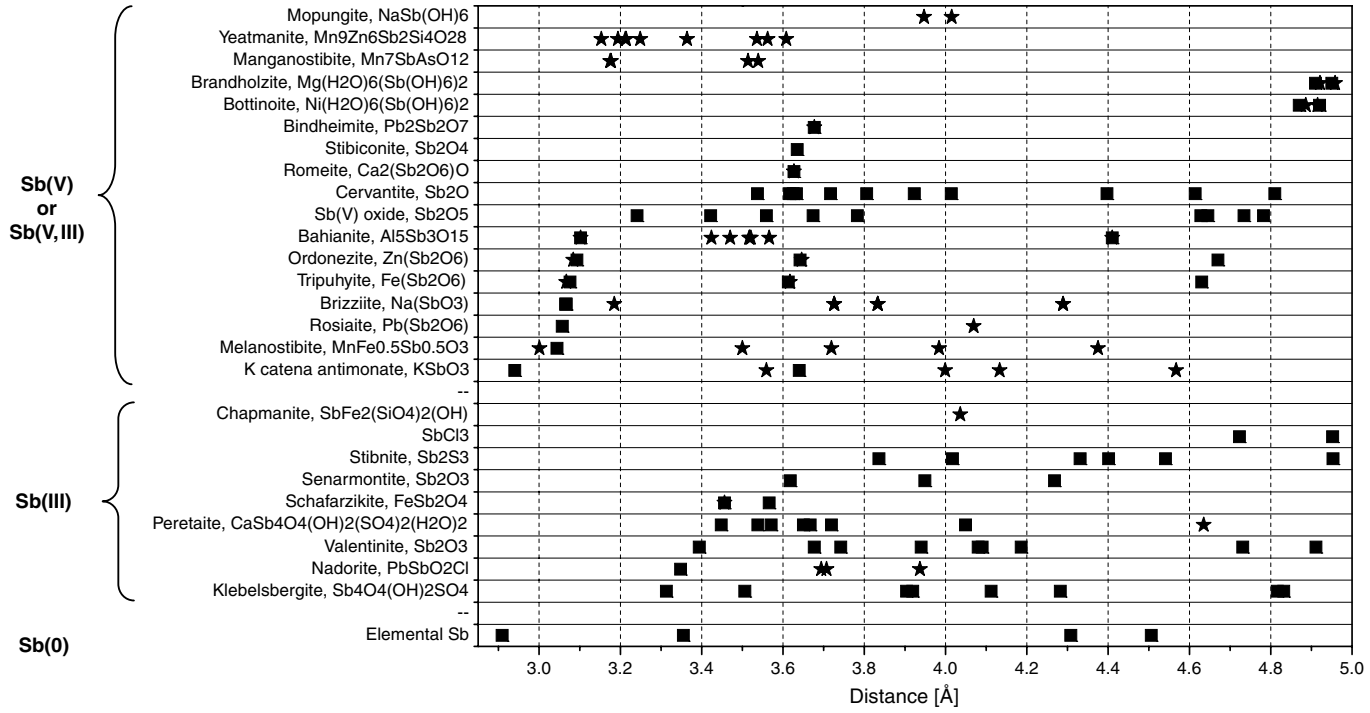

Fig. 2. Radial distances between Sb atoms (squares) and between Sb and other major atoms (stars) in Sb minerals and solids. The reference phases are grouped according to oxidation state and then sorted along the distances of next-nearest neighbor atoms.

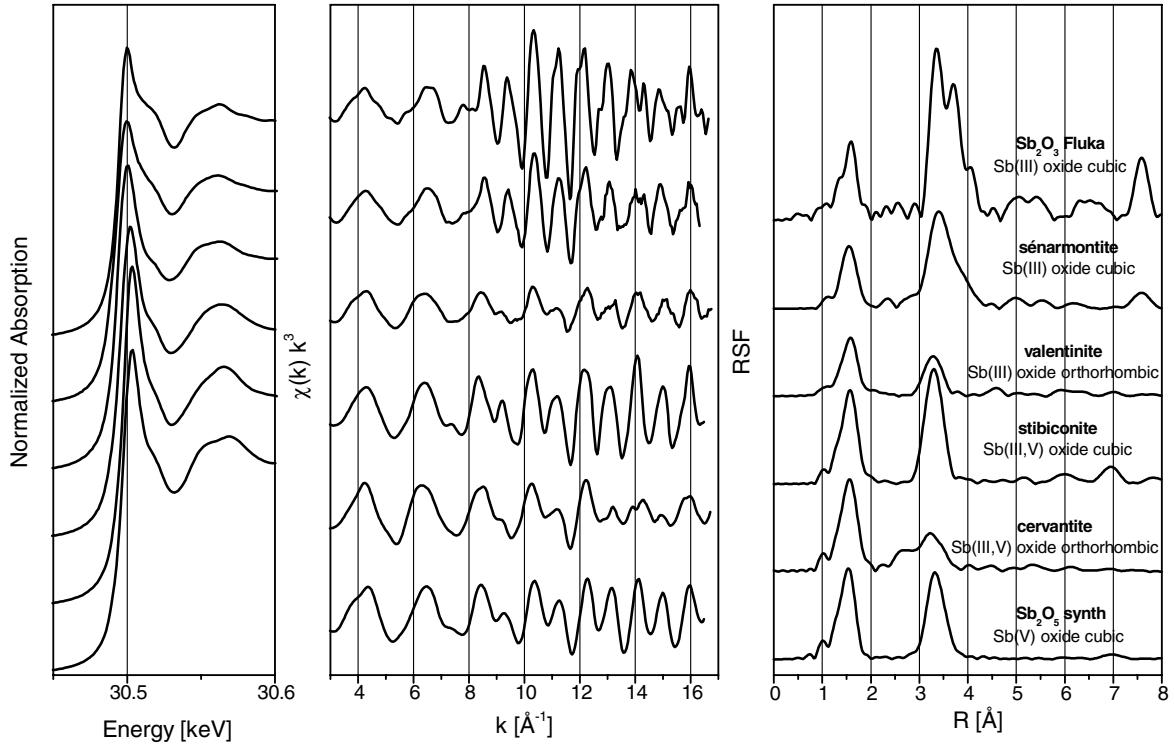

Fig. 3. Sb K-edge XAS spectra of Sb(III), Sb(III,V) and Sb(V) oxides.

about 1.6 Å not corrected for phase shift) and by fitted O-coordination numbers close to three (Table 2). The pentavalent Sb oxide shows a larger O-peak and a coordination number close to six. Of the mixed oxides, only stibiconite has an intermediate O-coordination number of 4.7, while that of cervantite is close to six. These results confirm that the tri- and pentavalent oxidation states of Sb can be reliably discriminated based on a difference of 4 eV at the absorption edge and based on their O-coordination numbers.

Table 2
XAS results of Sb(III), Sb(III,V) and Sb(V) oxides in comparison with their crystallographic structure

Sample	Formula	E_0 (eV)	Coordination shell			Metal shells			ΔE_0[a] (Å)	$\chi^2_{res\%}$[b]	Coord. shell XRD		Metal shells XRD	
			CN[c]	R[d] (Å)	σ^2[e] (Å^2)	CN	R (Å)	σ^2 (Å^2)			CN	R (Å)	CN	R (Å)
Sb^{III}oxide (Fluka)	Sb_2O_3 cubic	30,493	3.3 O	1.99	0.0023	4.7 Sb	3.65	0.0021[f]	12.5	7.4	3 O	1.98	3 Sb	3.62
			2.7 O	2.90	0.0050	4.9 Sb	3.95	0.0021[f]			3 O	2.92	6 Sb	3.95
						3.0 Sb	4.25	0.0021[f]					3 Sb	4.27
Sénarmontite	Sb_2O_3 cubic	30,493	3.3 O	1.97	0.0027	4.0 Sb	3.63	0.0032[f]	16.0	4.0	3 O	1.98	3 Sb	3.62
			2.4 O	2.88	0.0073	3.0 Sb	3.92	0.0032[f]			3 O	2.92	6 Sb	3.95
						2.2 Sb	4.23	0.0032[f]					3 Sb	4.27
Valentinite	Sb_2O_3 orthorhombic	30,493	3.4 O	1.98	0.0030	0.5 Sb	3.41	0.0025[f]	7.1	7.3	3 O	1.98–2.02	2 Sb	3.39
						1.4 Sb	3.62	0.0025[f]					2 Sb	3.68–3.74
													6 Sb	3.94–4.09
Stibiconite	Sb_2O_4 cubic	30,496	4.7 O	1.96	0.0021	3.9 Sb	3.62	0.0016	1.0	12.3	6 O	2.02	12 Sb	3.64
						5.5 Sb	6.32	0.0052					6 Sb	5.15
						8.9 Sb	7.35	0.0035					24 Sb	6.30
													12 Sb	7.28
Cervantite	Sb_2O_4 orthorhombic	30,497	5.9 O	1.98	0.0033	0.4 Sb	3.08	0.0020	5.9	10.5	6 O	1.93–2.02	3 Sb	3.54
						0.4 Sb	3.37	0.0024[f]					2 Sb	3.61–3.64
						1.4 Sb	3.63	0.0024[f]					5 Sb	3.91–4.02
											3 O	1.86–2.17	2 Sb	3.42
													1 Sb	3.54
													7 Sb	3.61–4.02
Sb^V oxide	Sb_2O_5 cubic	30,497	5.6 O	1.95	0.0034	4.0 Sb	3.62	0.0031[f]	3.9	5.7	3 O	2.04	3 Sb	3.32
						1.8 Sb	3.83	0.0031[f]			3 O	2.39	6 Sb	3.62
													3 Sb	3.90
													3 Sb	4.91

[a] Phase shift.
[b] Fit error.
[c] Coordination number and element.
[d] Radial distance.
[e] Debye–Waller factor.
[f] Parameter correlated during EXAFS fit.

Only the Fourier transform of the well crystalline, cubic Sb(III) oxide (Fluka) shows the expected splitting of the first metal coordination shell (3–4 Å, not corrected for phase shift) into three subshells, corresponding to 3 Sb at 3.62 Å, 6 Sb at 3.95 Å, and 3 Sb at 4.27 Å (Fig. 3) (Svensson, 1975). A reliable EXAFS fit of these three subshells was possible when the Debye–Waller factors were fitted as correlated variables. In comparison to the synthetic Sb(III) oxide, the Fourier transform of the natural, cubic Sb(III) oxide sénarmontite is less resolved. Nevertheless, three Sb distances could be reliably fitted. In the orthorhombic Sb(III) oxide valentinite, each Sb^{3+} is surrounded by 10 Sb atoms at distances of 3.39, 3.68, 3.74, 3.94 and 4.09 Å (Svensson, 1974). Of these 5 Sb distances, only the first two at 3.41 and 3.62 Å could be fitted.

The cubic Sb(III,V) oxide stibiconite has a pyrochlore-like structure with Sb^{3+} in pyramidal and Sb^{5+} in octahedral coordination (Dihlstroem and Westgren, 1937). Both Sb^{5+} and Sb^{3+} centers are surrounded by an identical arrangement of 4 Sb distances out to 7.28 Å (Table 2). The EXAFS fit shows three of these distances. The largest distance of 7.35 Å could be fitted, while an intermediate one expected at 5.15 Å could not be fitted. In the orthorhombic mixed oxide cervantite, the Sb^{3+} and the Sb^{5+} centers are surrounded by 10 Sb atoms at various distances between 3.42 and 4.02 Å (Thornton, 1977). Only 2 Sb atoms at the short distances of 3.37 and 3.63 Å, representing most likely the next metal neighbors of Sb^{3+} and Sb^{5+}, respectively, were detected by EXAFS. An additional Sb distance of 3.08 Å could be attributed to an ordoñezite impurity in the sample detected by XRD. This impurity may be responsible for the prevalence of pentavalent Sb as indicated by edge energy and O-coordination number (see above).

Cubic Sb_2O_5 has not been found in nature, but was used as the only available standard for pure Sb(V) oxide. Each Sb atom is surrounded by 15 Sb atoms at the distances 3.32, 3.62, 3.90 and 4.91 Å. Although XRD confirmed the phase identity and revealed a high crystallinity, only two Sb distances of 3.62 and 3.83 Å could be determined by EXAFS, while the shortest and the longest distances are missing.

Only for the two cubic Sb(III) oxides the structural determination by EXAFS was completely successful, including approximately correct coordination numbers for the metal shells. For the other oxides, metal shell coordination numbers were generally too small, and some shells were completely missing. The causes of these significant differences between crystallographic data and EXAFS spectroscopy are not clear at this time.

3.1.2. Antimonates

Fig. 4 and Table 3 give the XANES and EXAFS spectra and fit results of Sb(V) antimonates, which are likely to form in shooting-range soils due to their composition (except for the Na antimonate brizziite). All XANES spectra reveal a similar shape of the white line and an edge energy of 30,497 eV consistent with a pentavalent oxidation state of Sb. Both bindheimite (Gasperin, 1955) and roméite (Natta, 1933) have a pyrochlore-type structure and similar EXAFS spectra (like the third pyrochlore-type structure stibiconite shown again for comparison). The tunnels formed by $Sb(V)O_6$-octahedra are occupied by Pb and Ca, respectively. Indicative of the excellent quality of the EXAFS spectra, path lengths beyond 7 Å could be fitted, and distances are generally consistent with the crystallographic values. However, we could fit neither the two shells consisting solely of Pb and Ca, respectively, nor the contribution of these two atoms to the mixed Sb/Pb or Sb/Ca shells. In the Fe antimonate tripuhyite, which has a rutile-type structure (Bystroem et al., 1942), Sb is surrounded by one Fe and one Sb atom at a distance of 3.07–3.08 Å, and by 4 Fe and 4 Sb atoms at 3.61–3.62 Å. Hence, the two FT peaks at 2.6 and 3.2 Å (uncorrected for phase shift) arise each from two types of atoms, Sb and Fe. A fit with free running values for distances, coordination numbers and Debye–Waller terms resulted in physically meaningless values, requiring fit constraints. Hence the ratio of Fe/Sb coordination numbers was fixed at 1, based on the observation that the deviations from this ratio are generally to small to be detected by EXAFS-derived coordination numbers (Berlepsch et al., 2003). Furthermore, the Debye–Waller terms for both Sb shells and for both Fe shells were correlated. With these constraints a reliable fit was achieved. The distances of 3.06 and 3.59 Å for Fe atoms and of 3.09 and 3.56 Å for Sb atoms deviate only slightly from published XRD data, and the coordination numbers are in agreement with the XRD data (Table 3).

The Al, Cu and K antimonate samples have a very low crystallinity, which prevented the unequivocal phase identification by XRD. The Al antimonate has three broad peaks at around 27, 35 and 55°2θ (Cu radiation), in line with the rutile-like structures of tripuhyite, ordoñezite and squawcreekite. The XRD patterns of the Cu antimonate and K antimonate sample are similar, but due to even wider lines the peaks at 27 and 35°2θ fall together, hence their patterns revealed only two broad lines. The EXAFS spectra of these three samples are close to that of tripuhyite, suggesting a similar local structure. In line with this observation, two similar Sb distances could be fitted, while it was not possible to determine the position of Al, Cu and K, respectively.

In the ilmenite-like structure of brizziite, $Na(SbO_3)$, sheets of edge-sharing SbO_6 octahedra alternate with similar sheets of NaO_6-octahedra (Olmi, 1994). The EXAFS data of the oxygen coordination shell (6 O at 1.99 Å) and those of the first metal shell (3 Sb at 3.07 Å) are in agreement with the corresponding XRD values. The following Na atoms (1 Na at 3.19 Å, 3 Na at 3.73 Å, 3 Na

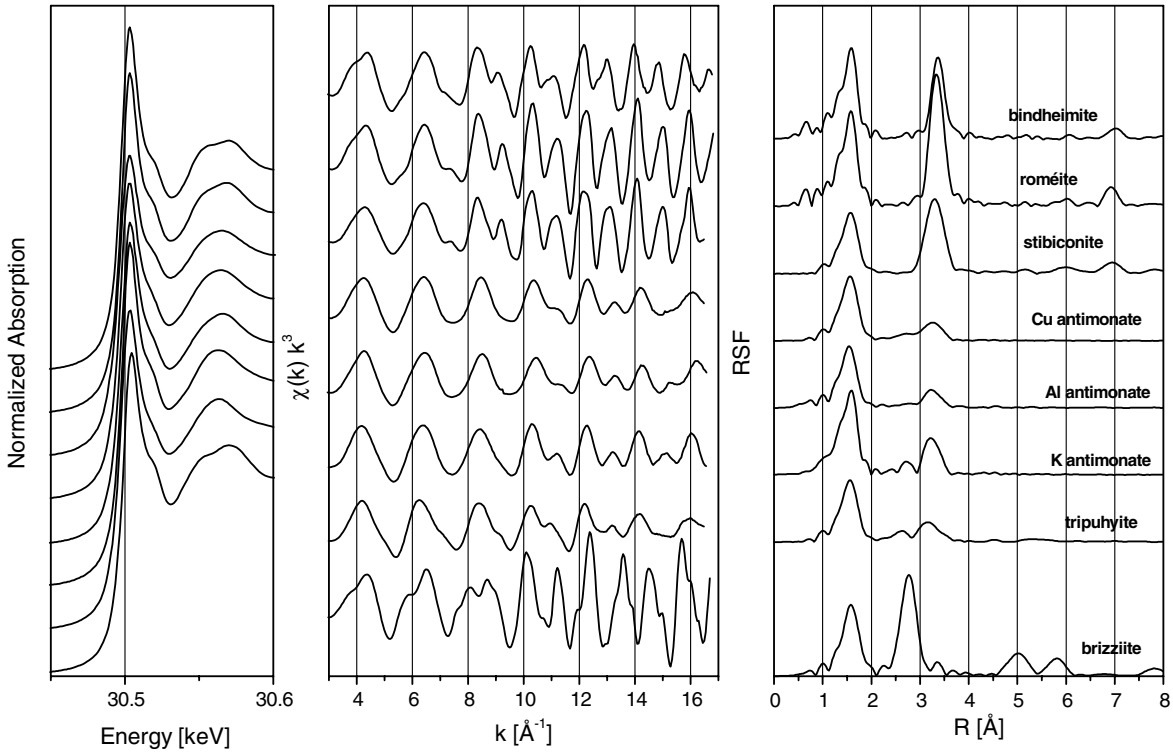

Fig. 4. Sb K-edge XAS spectra of pentavalent antimonates.

Table 3
XAS results of Sb(V) antimonates in comparison with their crystallographic structure

Sample	Formula	E_0 (eV)	Coordination shell			Metal shells			ΔE_0 (Å)	$\chi^2_{res\%}$	Coord. shell XRD		Metal shell XRD	
			CN	R (Å)	σ^2 (Å^2)	CN	R (Å)	σ^2 (Å^2)			CN	R (Å)	CN	R (Å)
Bindheimite synthetic	$Pb_2(Sb_2O_6)O$	30,497	5.7 O	1.97	0.0023	3.3 Sb	3.65	0.0023	4.6	23.2	6 O	2.00	12 Pb,Sb	3.68
						2.0 Sb	6.40	0.0047					6 Pb	5.20
						6.8 Sb	7.34	0.0039					24 Pb,Sb	6.37
													12 Sb	7.35
Roméite synthetic	$Ca_2(Sb_2O_6)O$	30,497	5.9 O	1.96	0.0023	5.3 Sb	3.63	0.0021	4.8	13.2	6 O	2.11	12 Ca,Sb	3.63
						7.1 Sb	6.34	0.0069					6 Ca	5.13
						13.5 Sb	7.37	0.0051					24 Ca,Sb	6.28
													12 Sb	7.25
Cu antimonate		30,497	6.1 O	1.97	0.0031	0.3 Sb	3.10	0.0022	5.0	6.9				
						1.6 Sb	3.60	0.0034						
	$Al_2(Sb_2O_6)_3$	30,497	6.0 O	1.96	0.0035	0.4 Sb	3.10	0.0042	3.7	7.6				
						1.0 Sb	3.57	0.0020						
K antimonate	$K(SbO_3)$	30,497	6.0 O	1.97	0.0028	1.1 Sb	3.07	0.0028	3.3	8.4				
						1.6 Sb	3.60	0.0067						
Tripuhyite synthetic	$FeSbO_4$	30,497	6.1 O	1.98	0.0035	0.8 Fe[a]	3.06	0.0031[a]	5.6	4.4	6 O	1.97–1.99	1Fe	3.07
						0.8 Sb[a]	3.09	0.0072[b]					1 Sb	3.08
						3.6 Fe[b]	3.59	0.0031[a]					4 Fe	3.62
						3.6 Sb[b]	3.56	0.0072[b]					4 Sb	3.61
Brizziite synthetic	$Na(SbO_3)$	30,497	6.0 O	1.99	0.0024	2.7 Sb	3.07	0.0013	5.1	5.5	6 O	1.97–2.01	3 Sb	3.07
						10.2 Na	3.77	0.0087					6 Na	3.73–3.83
						2.6 Sb	5.30	0.0006					6 Sb	5.30
						4.3 Sb	6.11	0.0018					9 Sb	6.13

[a,b] Parameters correlated during fit.

at 3.83 Å) are lumped together to one Na peak, which could be fit with 10 Na atoms at 3.77 Å. Antimony atoms as far as 5.30 and 6.13 Å could be fitted, again in excellent agreement with the XRD data.

3.1.3. Sorption complexes

Fig. 5 and Table 4 show the XANES and EXAFS spectra and fit results of Sb(III) and Sb(V) sorption complexes with likely sorbents in soils, goethite and humic acid. The XANES shape and edge position (30,497 eV) of Sb^{5+} sorbed to goethite, and its O-coordination number of six confirm the conservation of the pentavalent oxidation state; likewise, the edge energy of 30,493 eV and the coordination number close to three confirm conservation of the trivalent oxidation state after sorption. The edge energy and coordination number of the mixed Sb^{5+}/Sb^{3+} sorption sample are intermediate. The Fourier transforms of Sb(V) goethite and of Sb(V, III) goethite show a small backscat-

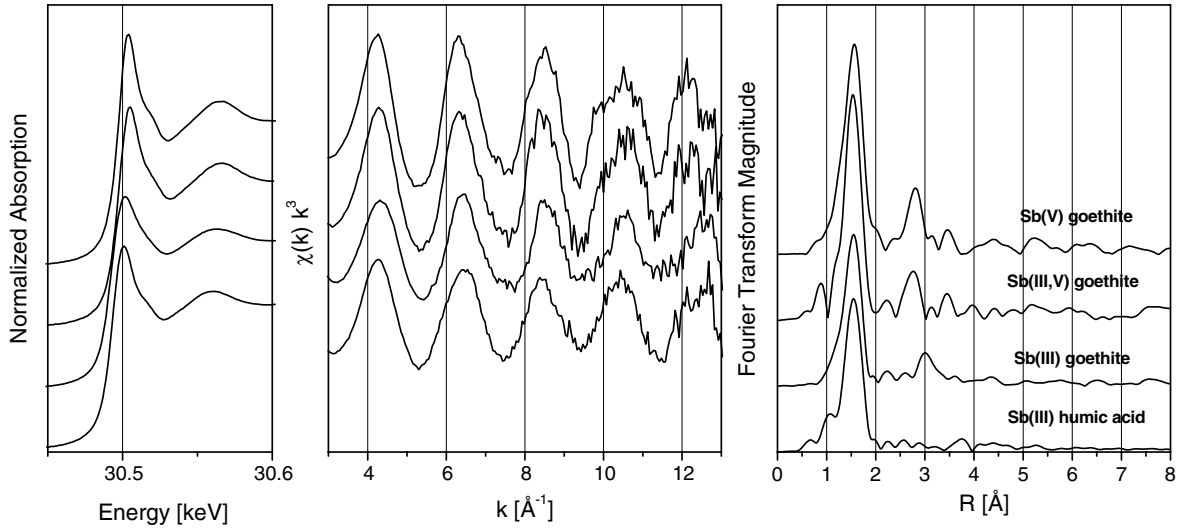

Fig. 5. Sb K-edge XAS spectra of sorption samples.

Table 4
XAS results of Sb(V) and Sb(III) sorption species

Sample	E_0 (eV)	Coordination shell			Metal shell			ΔE_0 (Å)	$\chi^2_{res\%}$
		CN	R (Å)	σ^2 (Å^2)	CN	R (Å)	σ^2 (Å^2)		
Sb(V) goethite	30,497	6.1 O	1.99	0.0042	1.0 Fe	3.08	0.0030	7.7	9.2
Sb(III,V) goethite	30,494	5.2 O	1.97	0.0031	0.9 Fe	3.09	0.0030	6.9	9.8
Sb(III) goethite	30,493	3.7 O	1.96	0.0035	1.9 Fe	3.46	0.0072	8.1	10.3
Sb(III) humic acid	30,492	3.7 O	1.98	0.0031				8.7	10.0

tering peak at 2.8 Å (uncorrected for phase shift), which was fitted with one Fe atom at a distance of 3.08–3.09 Å. This distance is in line with an $Sb(OH)_6$ octahedron sharing an edge with an $Fe(OH)_6$ octahedron, hence suggesting formation of edge-sharing innersphere sorption complexes at the goethite surface. For Sb(III) goethite, the Fourier transform peak is at 3.0 Å, corresponding to a fitted distance of 3.46 Å. This distance and the coordination number of two suggests formation of a bidentate, corner-sharing complex. Finally, the Sb(III) humic acid does not reveal any backscattering peaks beyond that of the O-coordination sphere. Assuming the complexation of the Sb(III) ion with carboxylate groups of humic acid, the backscattering signals of C atoms at a distance of 3–3.5 Å would be expected. The absence of such a peak may indicate that a substantial amount of Sb^{3+} remained as aqueous $Sb(OH)_3^0$ complex rather than being sorbed. However, an ill-defined distance of the binding C groups as well as the generally weak backscattering of C may mask existing complexation (Schmeide et al., 2003).

3.2. Antimony speciation of soil samples

3.2.1. Iterative target test factor analysis

The EXAFS spectra of soil samples are shown in Fig. 6 (full lines). The k^3-weighted EXAFS spectra and Fourier transforms shown in the upper part (Losone) reveal heavy backscatterers at long distances, which indicates the presence of a solid Sb phase. The spectra in the lower part (Zuchwil, Goldau), are dominated by backscattering from the first coordination sphere (low frequency oscillations) with only a minor influence of backscattering atoms beyond the coordination sphere. Fourier transform peak heights of the first coordination shell (at ≈1.5 Å, uncorrected for phase shift) increase from top to bottom, while those of more distant shells (at 2.7, 3.2, 4.0 Å) decrease. Differences between samples are gradual, suggesting variable mixtures of several species.

In order to determine the number of spectral components necessary to reconstruct the sample spectra, we performed an Eigenanalysis using the ITFA program

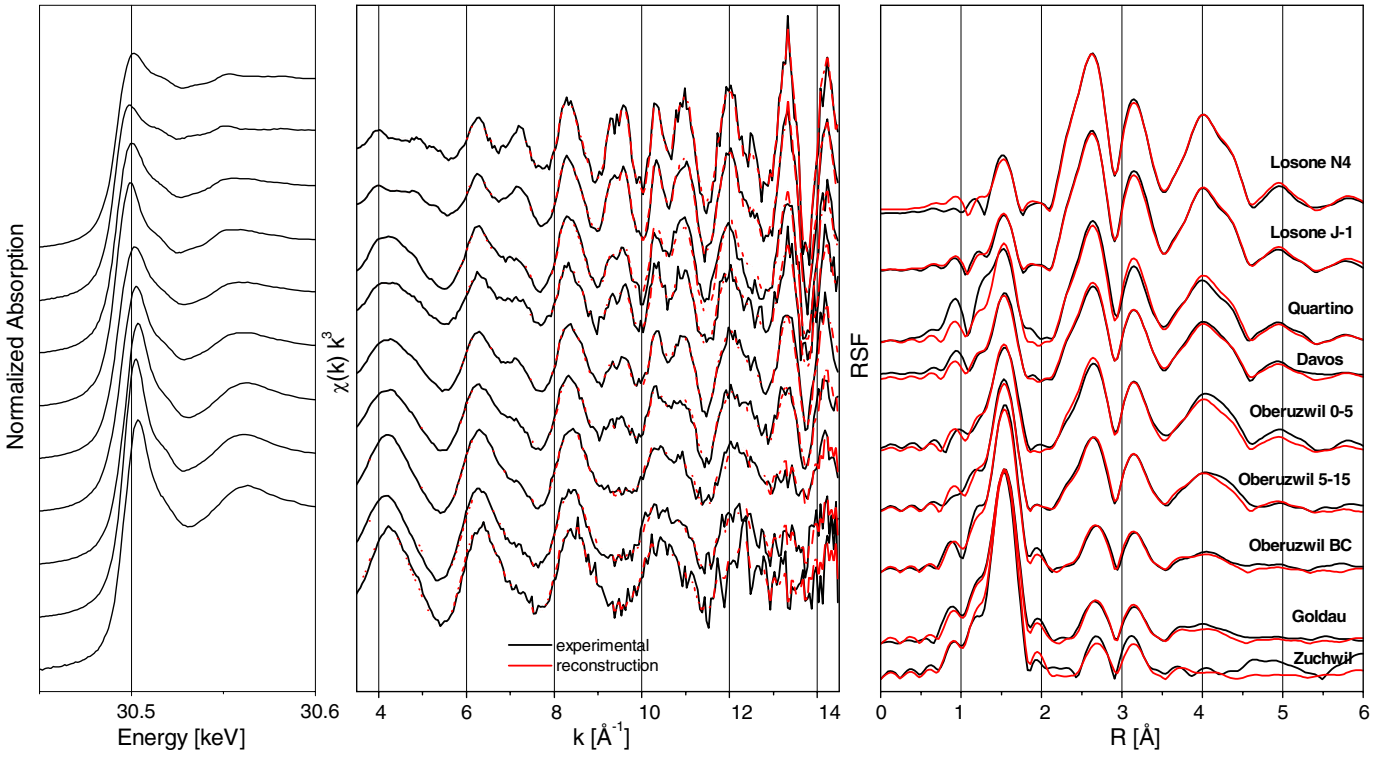

Fig. 6. Sb K-edge XAS spectra of the soil samples from six different shooting ranges (black lines), and their reconstruction with two principal components (red lines, only EXAFS spectra and their Fourier transforms).

package (http://www.esrf.fr/UsersAndScience/Experiments/CRG/BM20/Software/). The indicator value reached a minimum for 2 components, suggesting that all nine spectra are mixtures of two spectral components (not shown). In line with this, only the first two Eigenvectors show strong EXAFS oscillations, while the small amplitudes of the next two Eigenvectors reveal their weak contribution to the spectral reconstruction (Fig. 7). In addition to the statistical noise characterized by high frequencies, the Eigenvectors 3 and 4 contain also smaller frequencies typical for EXAFS spectra (Fig. 7, left). The Fourier transforms of these Eigenvectors support, however, that these frequencies do not arise from additional backscattering shells not already accounted for by Eigenvectors 1 and 2. The Fourier Transform magnitude peaks especially of Eigenvector 3 follow largely those of Eigenvector 2, suggesting that they are due to small variations of the amplitudes of the backscattering waves, which may be generated by small variations of coordination numbers, structural disorder and/or by variations of the spline background subtraction. Finally, deviations between experimental spectra (black lines in Fig. 6) and the reconstructions based on two components (red lines in Fig. 6) are very small. In fact, the reconstructions appear as noise-filtered spectra (see also Fig. 8). In conclusion, the statistical and visual analysis of the nine spectra strongly suggests that only two systematic spectral components are present, hence all nine samples contain variable ratios of only two chemical species.

Component 1 showed a maximum abstract concentration for sample Losone N4, while component 2 showed a maximum abstract concentration for sample Zuchwil. Assuming that these components represent the relatively pure species, we performed VARIMAX rotation and iterative target test. The output of this procedure are the spectral representations of the two components, i.e., the spectra of the two species (Fig. 8), and the relative concentrations of both components in the samples, i.e., their speciation (Table 5).

3.2.2. Species identification

Fig. 8 shows the spectral representations of species 1 and 2 in comparison to the spectra of the soil samples with the purest occurrence of each species (Losone N4 and Zuchwil, respectively), and in comparison to the most similar reference spectra. The spectrum of species 1 contains most spectral features of Losone N4 with two exceptions: a Fourier transform peak at 1.6 Å indicative of an O-coordination shell is missing, while all other peaks are more pronounced. A comparison with species 2 demonstrates that these differences are due to the spectral mixture of species 1 and 2 in sample Losone N4 (Table 5).

Of all references, the spectrum of species 1 is closest to that of metallic Sb (Fig. 8). The multi-shell fit confirms that in species 1 each Sb is surrounded solely by other Sb atoms at distances consistent with those of a metal reference foil measured in transmission mode (Table 6) and with crystallographic structure data (Fig. 2) (Barrett et al., 1963). For both, species 1 and the reference foil, the EXAFS-derived coordination numbers of the first two shells are below the expected value of 3. However, the close agreement of the spectral features and the fitted structure data of species 1 and the reference foil demonstrate unequivocally that species 1 is metallic Sb.

The spectral representation of species 2 is, apart from less noise, almost identical to that of sample Zuchwil, in line with the pure composition of this soil sample (Fig. 8, Table 5). The edge energy of sample Zuchwil (30,497 eV) suggests a pentavalent oxidation state. Of all available reference spectra, the spectrum of species 2 is most similar to Sb(V) sorbed to goethite, and to the Fe antimonate tripuhyite. The most significant difference between species 2

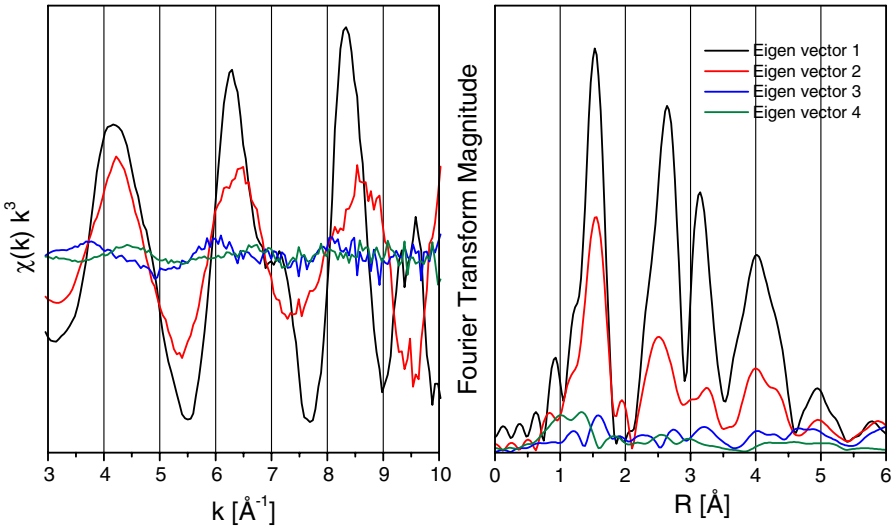

Fig. 7. Eigenvector analysis of the Sb K-edge EXAFS spectra of the nine soil samples (see Fig. 6). Shown are the first four Eigenvectors and their Fourier Transforms.

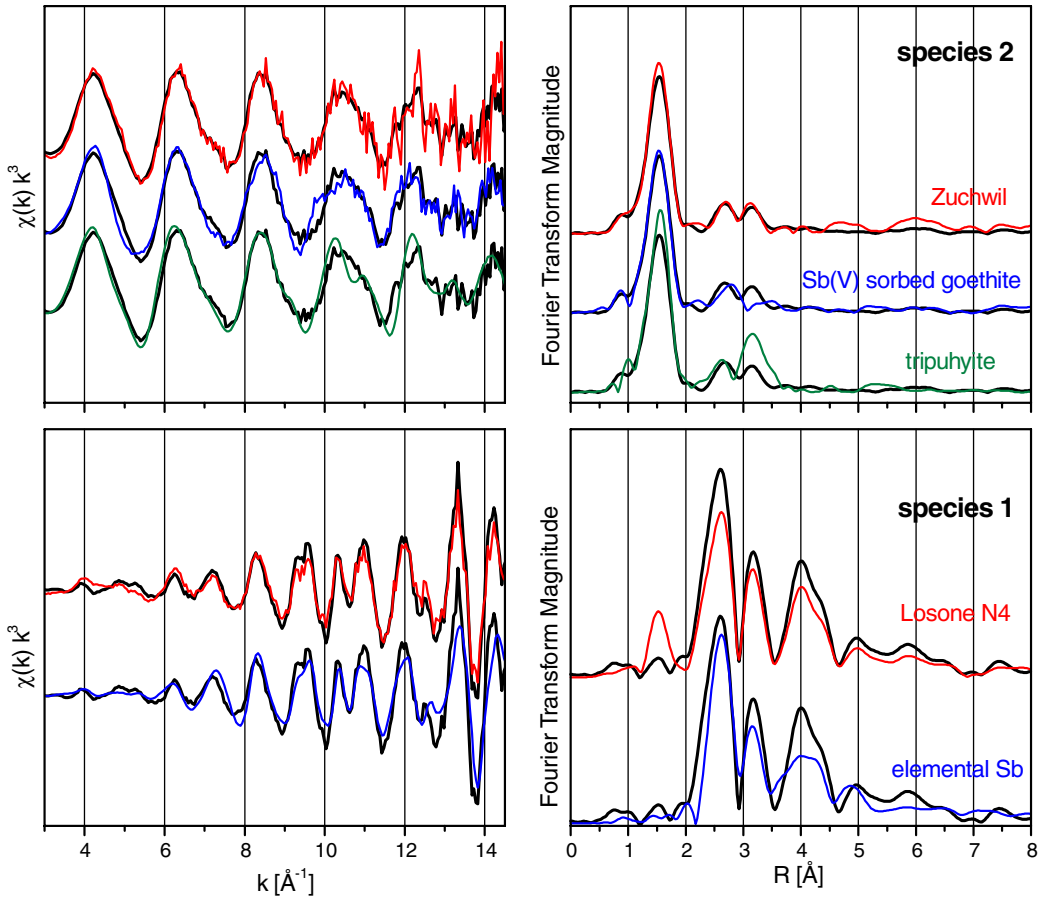

Fig. 8. ITFA-derived Sb K-edge EXAFS spectra of the two Sb species in the soil samples (black lines). For comparison are shown the experimental spectra of the soil samples with the largest fraction of the respective species (red), and of selected reference species (blue and green).

Table 5
Fractional distribution of the two Sb species in the soil samples and edge energy of the XANES spectra

Sample	Species 1	Species 2	Sum	E_0 (eV)
Losone N-4	0.75	0.26	1.01	30,491
Losone J-1	0.64	0.29	0.93	30,493
Quartino	0.50	0.52	1.02	30,493
Davos	0.41	0.44	0.85	30,493
Oberuzwil 0–5	0.37	0.55	0.92	30,494
Oberuzwil 5–15	0.25	0.66	0.91	30,495
Oberuzwil BC	0.07	0.84	0.92	30,496
Goldau	0.04	0.90	0.94	30,497
Zuchwil	0.00	1.00	1.00	30,497

and these references is the absence of a Fourier transform peak at 3.2 Å for the sorption sample, and its more pronounced expression for tripuhyite, suggesting an intermediate local structure for species 2.

To elucidate the structure of species 2, multi-shell fit was performed. Antimony is octahedrally coordinated to O, corroborating the pentavalent oxidation state already suggested by the edge energy (Fig. 1, Table 2). The two small backscattering peaks in the Fourier transform at distances above 2 Å (Fig. 8, uncorrected for phase shift) were attempted to fit with Fe shells, Sb shells, Pb shells, and with combined Fe and Sb shells as performed for the tripuhyite sample. Only the fit with two Fe shells resulted in a good fit of the spectrum and in physically meaningful values of distance, coordination number, Debye–Waller factor and phase shift. The fitted distances of 3.10 and 3.56 Å together with coordination numbers of 0.9 and 1.4 (Table 6) suggest a local structure where an $Sb(O,OH)_6$ octahedron shares one edge with an $Fe(O,OH)_6$ octahedron, and simultaneously shares corners with one or two $Fe(O,OH)_6$ octahedra as shown in Fig. 9.

While the EXAFS fit results of Sb(V) sorbed to goethite reveal only the edge-sharing sorption complex (Table 4), higher surface loadings may cause the formation of corner-sharing in addition to edge-sharing complexes (Spadini et al., 1994). Furthermore, ferrihydrite exposing a higher variety of surface sites as compared to goethite tends to form both types of sorption complexes, as has been demonstrated for Cd, Se and As (Manceau and Charlet, 1994; Spadini et al., 1994). If the ratio of the fractions of edge and corner-sharing arrangements would change between samples, a total of three different species would have been observed by ITFA (including the metal species). Since this was not the case, both arrangements seem to occur at the same ratio in all samples in spite of the wide range of pH, Sb concentration and other physicochemical soil parameters (Table 1). This suggests that the formation of

Table 6
Local structure of species 1 and 2 and of Sb(0) metal

Sample	Coordination shell			Metal shells			ΔE_0 (eV)	$\chi^2_{res\%}$
	CN	R (Å)	σ^2 (Å^2)	CN	R (Å)	σ^2 (Å^2)		
Species 1	2.1 Sb	2.90	0.0013	2.1 Sb	3.35	0.0027	6.6	7.5
				6.7 Sb	4.30	0.0045		
				6.1 Sb	4.51	0.0039		
Sb metal	1.8 Sb	2.91	0.0014	2.4 Sb	3.33	0.0021	9.2	11.3
				5.7 Sb	4.29	0.0048		
				6.1 Sb	4.49	0.0060		
Species 2	5.4 O	1.98	0.0033	0.9 Fe	3.10	0.0036	7.6	4.4
				1.4 Fe	3.56	0.0039		

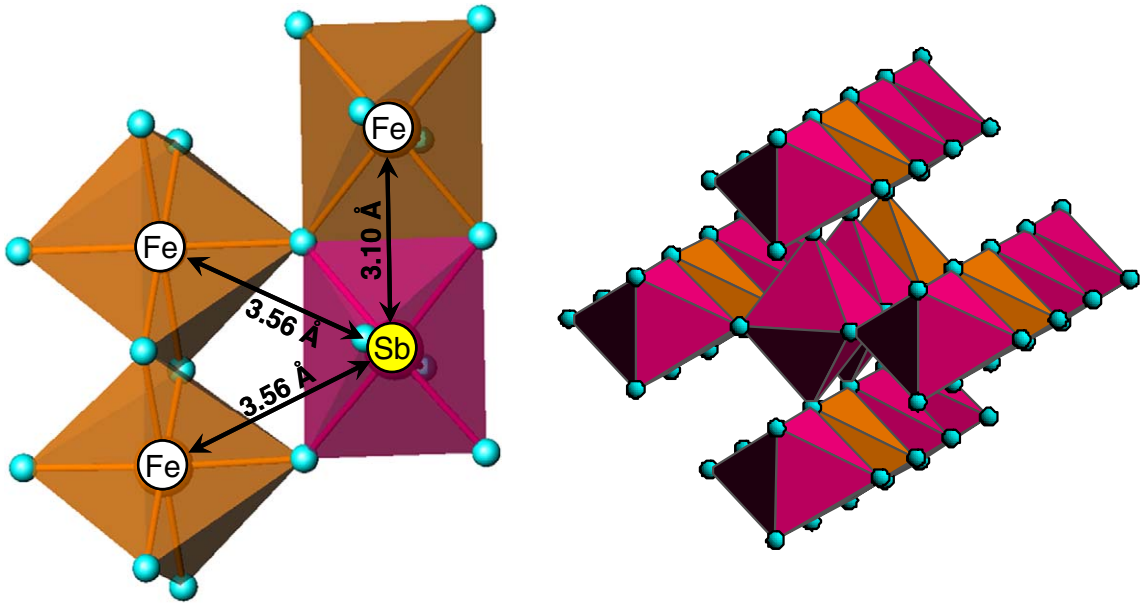

Fig. 9. Structural model of species 2 (left) and of tripuhyite, $Fe^{III}Sb^{V}0_4$ (right). Sb octahedra are shown in pink, Fe octahedra in orange.

both sorption complexes is controlled by surface sites, indicative of preferential sorption to ferrihydrite rather than to more crystalline goethite (Manceau and Charlet, 1994).

An alternative explanation would be the formation of a solid Sb and Fe hosting phase like the Fe antimonate tripuhyite, $FeSbO_4$. In this structure, SbO_6 and FeO_6 octahedra share edges along the chains, and corners between chains, revealing a structural arrangement similar to that of species 2 (compare both structures in Fig. 9). The distances of first (3.06–3.08 Å) and second metal shells (3.61–3.63 Å) reported for several tripuhyite samples are in fact similar to those of species 2 (Berlepsch et al., 2003). However, a fit of both Sb—Fe and Sb—Sb backscattering paths as in tripuhyite failed, and only Fe backscattering paths could be reliably fitted. To further confirm the absence of backscattering Sb atoms, we performed a comparative wavelet analysis of the spectra of species 2 and tripuhyite, following the procedure developed by Funke et al. (2005). The detail wavelet plots of the radial distances $2.4 \leqslant r \leqslant 3.5$ Å using the optimized Morlet parameters $\eta = 6$ and $\sigma = 1$ revealed only a peak at smaller k indicative of Fe, but no peak at higher k indicative of Sb for species 2, hence the presence of Sb backscatterers can be excluded (data not shown). While one could assume that the structure of species 2 represents small clusters of an Fe-rich tripuhyite, based on the small coordination numbers for the second metal shell and on the prevalence of Fe neighbors, the tripuhyite samples investigated by Berlepsch et al. (2003) show only a small deviation from the ideal Fe-to-Sb ratio of one (site occupancy factor, SOF, of Sb: 0.47–0.53). Furthermore, our attempts to synthesize an antimonate with less Sb (SOF < 0.4) failed and led to the precipitation of Fe and Sb oxides as separate phases. Therefore, we have to reject the hypothesis that species 2 is tripuhyite of low crystallinity.

However, it cannot be excluded that species 2 is Sb(V) occluded in the structure of an Fe oxide rather than being Sb(V) sorbed to Fe oxide surfaces. In the case of *independent* edge and corner-sharing sorption complexes with Fe coordination numbers of 1 and 2, respectively, the spectral mixture of both complexes should result in fitted coordina-

tion numbers of 0.5 and 1.0, while they are in fact 0.9 and 1.4. Hence the higher coordination numbers may suggest formation of such an occlusion, but—considering the large error observed for some of references—cannot prove it.

In conclusion, two types of sorption complexes, edge-sharing and corner-sharing, occurring in about equal proportions in all samples, are the most consistent interpretation of species 2.

3.2.3. Quantitative speciation and geochemical implications

The relative concentrations of Sb(V) sorbed to Fe oxides and of metallic Sb as derived by ITFA are given in Table 6. The Sb(V) species is present in all samples, confirming the strong association between Sb(V) and Fe oxides suggested earlier by selective sequential extractions (Crecelius et al., 1975; Blay, 2000). Samples from Goldau and Zuchwil have the highest proportions of Sb(V).

The remaining sites, Davos, Quartino and Losone, have significant proportions of metallic Sb. This metallic Sb may stem from small fragments of unweathered bullet cores. Such bullet fragments could have formed through abrasive forces during bullet impact into the soil, and may not have been eliminated from the samples by sieving. This interpretation is consistent with a high percentage of Sb(0) in the Quartino sample, which has been collected from a stop butt constructed with ash-filled tires, and may have a smaller weathering potential than soil. It is also consistent with a small percentage of Sb(0) in a bullet crust collected at Oberuzwil (Oberuzwil BC), where metallic bullet parts could be easily separated. However, the very high percentage of Sb(0) in the Losone samples suggests a different scenario.

The Losone samples originate from behind the stop butts and contain significant quantities of chestnut leaf mould. The soil at this site is very acidic, organic matter-rich, and has a very low bulk density. Pb concentrations were as high as 80,900 mg kg^{-1} (Knechtenhofer et al., 2003). The surface of a bullet found at this site was bright-metallic from surface dissolution, and it did not show a weathering crust, suggesting rapid bullet weathering. This shooting range was only rarely used in the last 5 years before sampling, making the existence of small, unweathered bullet fragments unlikely. Pb L_{III}-edge XAS spectroscopy indicated that this sample does not contain Pb(0), but Pb(II), which is predominantly bound to soil organic matter (Fig. 10). The presence of Sb(0) and the absence of Pb(0) therefore strongly suggest, that metallic Sb(0) remained undissolved during Pb oxidative dissolution. In line with the standard reduction potentials of Sb

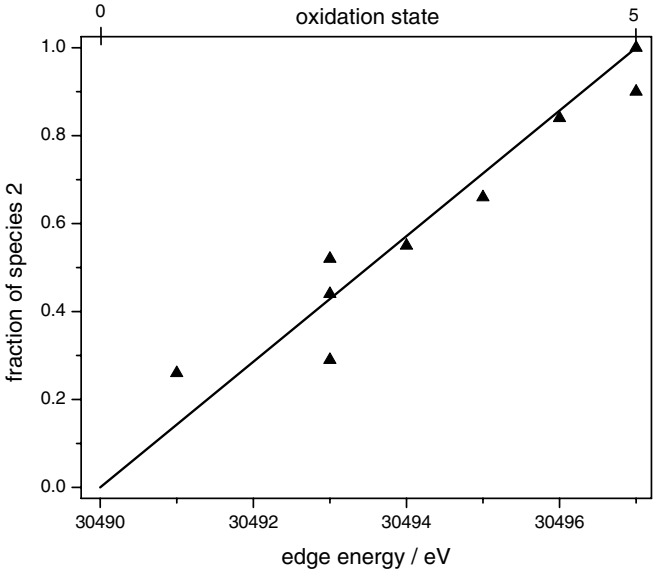

Fig. 11. XANES edge energies of soil samples in relation to the fraction of the Sb(V) species (species 2). The line connects the edge energies of metallic Sb(0) (30,490 eV) and of Sb(V) antimonate references (30,497 eV).

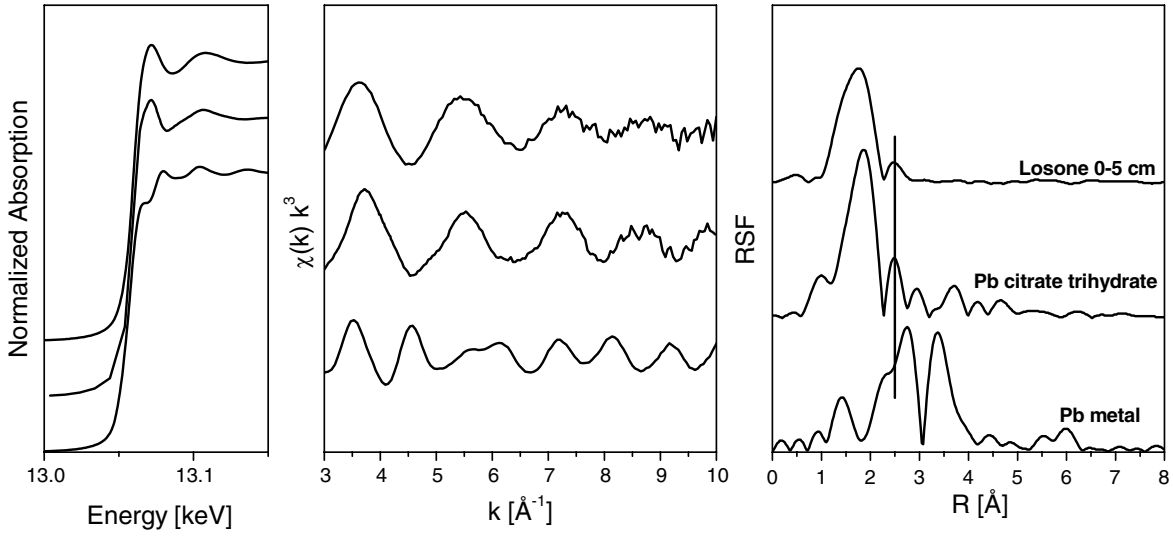

Fig. 10. Pb L_{III} edge EXAFS spectra of Losone topsoil in comparison to Pb citrate and metallic Pb(0). The marked second peak in the Fourier transform corresponds to 2 C atoms at a radial distance of 3.2 Å, in line with Pb bonding to carboxylate groups.

and Pb ($E^{\Theta} = 0.204$ V for Sb(0) → Sb(III), $E^{\Theta} = -0.125$ V for Pb(0) → Pb(II) at acidic pH), Sb(0) should act as an oxidizer for Pb(0), hence explaining why Sb(0) clusters within the PbSb alloy have a much higher resistance against weathering than the Pb(0) clusters. Considering the excess of Pb, even a reduction of already oxidized Sb seems to be possible.

No indication of a third, Sb(III) species was found by XAS spectroscopy and ITFA. According to our experience, the lower detection limit of ITFA for an additional species is 1–5%, considering the given spectral quality. Furthermore, the XANES edge energies of the soil samples do not show a systematic deviation from the line linking the energies of the Sb metal and antimonate references (Fig. 11). Hence a separate Sb(III) species, like Sb(III) complexed by soil organic matter, would account for less than 5%. While beam-induced sample oxidation was observed when collecting Sb L-edge XANES of some of the references at room temperature (data not shown), the higher energy of the Sb K-edge and the sample cooling to 20 K prevented redox changes. Hence oxidation or reduction of Sb(III) during the measurement can be excluded. Although substantial proportions of Sb(III) were found in oxalate extracts of some of the same samples investigated here (Johnson et al., 2005), more recent experiments suggest that oxalate releases not only Sb associated with amorphous Fe oxides, but dissolves Sb(0); hence the previously found Sb(III) may be an artifact of the extraction procedure. Therefore our results clearly demonstrate that Sb(III) species do not significantly contribute to the speciation of bulk soil. While Sb(III) may be formed as an intermediate product during the oxidation of Sb(0), the Sb(III) oxidation kinetics seem to be much faster in soils than in (oxic) surface waters, hence preventing the enrichment of Sb(III) (Filella et al., 2002; Leuz and Johnson, 2005). This difference between soils and waters might be explained by the redox-catalyzing surfaces present in many soils.

4. Conclusions

In spite of a substantial soil variation in terms of parent material, pH, Sb concentrations and range history, only two Sb species were found in shooting-range soils: first, Sb(V) sorbed to Fe oxides by forming both edge-sharing and corner-sharing inner-sphere sorption complexes. Second, metallic Sb(0), which may be part of unweathered bullet fragments. In one case, however, metallic Sb(0) remained even after complete oxidation of metallic Pb, pointing to a higher resistance of Sb(0) against weathering. The results show that Sb(V) is the prevailing oxidation state after weathering of metallic Sb(0) in oxic soils, while Sb(III) was not detected. In confirmation, a recent XANES investigation on soils contaminated by Sb and Sb_2O_3 smelter emissions showed also predominantly Sb(V) (Takaoka et al., 2005). Therefore, the more toxic Sb(III) seems to play only a minor role in oxic soils.

Acknowledgements

We would like to acknowledge V. Schärer, V. Galbier, G. Tognina, A. Tremp and Paul Wersin for making access to the Swiss shooting ranges possible. Reference minerals were provided by M.O. Figueiredo, Crystal and Mineral Centre, Lisboa, Portugal. The Sb^{3+} humic acid reference was prepared by J. Buschmann, EAWAG. XRD was performed by F. Prokert and A. Scholz, FZR. We thank Herman Moench (EAWAG) and Kurt Barmettler (ETHZ) for sample preparation and analysis. The final version of the manuscript benefited from the careful reviews by AE D.J. Vaughan, A. Manceau and two anonymous referees. This study was funded in part by the Swiss National Science Foundation.

Associate editor: David J. Vaughan

References

Adriano, D.C., 1986. *Trace Elements in the Terrestrial Environment*. Springer Verlag.

Ainsworth, N., Cooke, J.A., Johnson, M.S., 1990. Distribution of antimony in contaminated grassland. 1. Vegetation and soils. *Environ. Pollut.* **65**, 65–77.

Ankudinov, A.L., Rehr, J.J., 1997. Relativistic spin-dependent X-ray absorption theory. *Phys. Rev. B*, 56.

Anonymous. 1998. Vadose Zone Characterization Project at the Hanford Tank Farms: BX Tank Farm Report. GJO-HAN-19, U.S. Department of Energy, Grand Junction Project Office, Grand Junction, Colorado.

Anonymous. 2004. Inorganic Crystal Structure Database 2004-02. National Institute of Standards and Technology.

Barrett, C.S., Cucka, P., Haefner, K., 1963. Crystal structure of antimony at 4.2, 78 and 298 K. *Acta Crystallogr.* **16**, 451–453.

Basunia, S., Landsberger, S., 2001. Contents and leachability of heavy metals (Pb, Cu, Sb, Zn, As) in soil at the Pantex firing range, Amarillo, Texas. *J. Air Waste Manag. Assoc.* **51**, 1428–1435.

Berlepsch, P., Armbruster, T., Brugger, J., Criddle, A.J., Graeser, S., 2003. Tripuhyite, $FeSbO_4$, revisited. *Mineral. Mag.* **67**, 31–46.

Blay, K., 2000. Sorption wässriger Antimon-Spezies an bodenbildende Festphasen und Remobilisierung durch natürliche Komplexbildner. PhD Thesis, Technische Universität München.

Bunzl, K., Trautmannsheimer, M., Schramel, P., 1999. Partitioning of heavy metals in a soil contaminated by slag: a redistribution study. *J. Environ. Qual.* **28**, 1168–1173.

Bystroem, A., Hoek, B., Mason, B., 1942. The crystal structure of zinc metantimonate and similar compounds. *Arkiv foer Kemi, Mineralogi och Geologi, B* **15**, 1–8.

Calmano, W., Mangold, S., Welter, E., 2001. An XAFS investigation of the artefacts caused by sequential extraction analyses of Pb-contaminated soils. *Fresenius J. Anal. Chem.* **371**, 823–830.

Crecelius, E.A., Bothner, M.H., Carpenter, R., 1975. Geochemistries of arsenic, antimony, mercury, and related elements in sediments of Puget Sound. *Environ. Sci. Technol.* **9**, 325–333.

Dihlstroem, K., Westgren, A., 1937. Über den Bau des sogenannten Antimontetroxyds und der damit isomorphen Verbindung $BiTa_2O_6F$. *Z. Anorg. Allg. Chem.* **235**, 153–160.

Fahrenhorst, C., Renger, M., 1990. The effects of very large amounts of lead, antimony and arsenic in agricultural soils in the vicinity of shooting ranges. *VDLUFA Kongressberichte* **32**, 827–830.

Filella, M., Belzile, N., Chen, Y.-W., 2002. Antimony in the environment: a review focused on natural waters. I. Occurrence. *Earth-Sci. Rev.* **57**, 125–176.

Funke, H., Scheinost, A.C., Chukalina, M., 2005. Wavelet analysis of extended X-ray absorption fine structure data. *Phys. Rev. B* **71**, 094110.

Gasperin, M., 1955. Synthèse et identification de deux oxydes doubles de tantale et d'étain. *CR Hebd. Acad. Sci.* **240**, 2340–2342.

Giuseppetti, G., Tadini, C., 1973. Riesame della struttura cristallina della nadorite: $PbSbO_2Cl$. *Period. Mineral.* **42**, 335–345.

Johnson, C.A., Moench, H., Wersin, P., Kugler, P., Wenger, C., 2005. Solubility of antimony and other elements in samples taken from shooting ranges. *J. Environ. Qual.* **34**, 248–254.

Kim, N.D., Fergusson, J.E., 1991. Effectiveness of a commonly used sequential extraction technique in determining the speciation of Cd in soils. *Sci. Total Environ.* **105**, 191–209.

Knechtenhofer, L., 2002. Small scale variability of lead and other contaminants in a shooting-range soil: impact of preferential water flow. MS Thesis, Department of Environmental Sciences, ETH Zurich, 62.

Knechtenhofer, L.A., Xifra, I.O., Scheinost, A.C., Flühler, H., Kretzschmar, R., 2003. Fate of heavy metals in a strongly acidic shooting-range soil: small-scale metal distribution and its relation to preferential water flow. *J. Plant Nutr. Soil Sci.* **166**, 84–92.

Krachler, M., Emons, H., Zheng, J., 2001. Speciation of antimony for the 21th century: promises and pitfalls. *Trends Anal. Chem.* **20**, 79–90.

Krupka, K.M., Serne, R.J., 2002. *Geochemical Factors Affecting the Behavior of Antimony, Cobalt, Europium, Technetium, and Uranium in Vadose Sediments*. PNNL-14126, Pacific Northwest National Laboratory, Richland, Washington.

Legoux, Y., Blain, G., Guillaumont, R., Ouzounian, G., Brillard, L., Hussonnois, M., 1992. Kd measurements of activation, fission and heavy elements in water/solid phase systems. *Radiochim. Acta* **58/59**, 211–218.

Leuz, A.-K., Johnson, C.A., 2005. Oxidation of Sb(III) to Sb(V) by O_2 and H_2O_2 in aqueous solutions. *Geochim. Cosmochim. Acta* **69**, 1165–1172.

Manceau, A., Boisset, M.C., Sarret, G., Hazemann, J.L., Mench, M., Cambier, P., Prost, R., 1996. Direct determination of lead speciation in contaminated soils by EXAFS spectroscopy. *Environ. Sci. Technol.* **30**, 1540–1552.

Manceau, A., Charlet, L., 1994. The mechanism of selenate adsorption on goethite and hydrous ferric oxide. *J. Colloid Interface Sci.* **168**, 87–93.

Manceau, A., Lanson, B., Schlegel, M.L., Hargé, J.C., Musso, M., Eybert-Bérard, L., Hazemann, J.-L., Chateigner, D., Lamble, G.M., 2000. Quantitative Zn speciation in smelter-contaminated soils by EXAFS spectroscopy. *Am. J. Sci.* **300**, 289–343.

Mosselmans, J.F.W., Helz, G.R., Pattrick, R.A.D., Charnock, J.M., Vaughan, D.J., 2000. A study of speciation of Sb in bisulfide solutions by X-ray absorption spectroscopy. *Appl. Geochem.* **15**, 879–889.

Natta, G.B.M., 1933. Tetrossido di antimonio e antimoniati. *Zeitschrift für Kristallographie, Kristallgeometrie, Kristallphysik, Kristallchemie* **85**, 271–296.

Oelkers, E.H., Sherman, D.M., Ragnarsdottir, K.V., Collins, C., 1998. An EXAFS spectroscopic study of aqueous antimony(III)-chloride complexation at temperatures from 25 to 250 °C. *Chem. Geol.* **151**, 21–27.

Olmi, F.S.C., 1994. Brizziite, $NaSbO_3$, a new mineral from the Cetine mine (Tuscany, Italy): description and crystal structure. *Eur. J. Mineral.* **6**, 667–672.

Ressler, T., 1998. WinXAS: a program for X-ray absorption spectroscopy data analysis under MS-Windows. *J. Synchrotron Radiat.* **5**, 118–122.

Roberts, D.R., Scheinost, A.C., Sparks, D.L., 2002. Zn speciation in a smelter-contaminated soil profile using bulk and micro-spectroscopic techniques. *Environ. Sci. Technol.* **36**, 1742–1750.

Rossberg, A., Reich, T., Bernhard, G., 2003. Complexation of uranium(VI) with protocatechuic acid—application of iterative transformation factor analysis to EXAFS spectroscopy. *Anal. Bioanal. Chem.* **376**, 631–638.

Scheinost, A.C., Kretzschmar, R., Pfister, S., Roberts, D.R., 2002. Combining selective sequential extractions, X-ray absorption spectroscopy and principal component analysis for quantitative zinc speciation in soil. *Environ. Sci. Technol.* **36**, 5021–5028.

Scheinost, A.C., Rossberg, A., Marcus, M., Pfister, S., Kretzschmar, R., 2005. Quantitative zinc speciation in soil with XAFS spectroscopy: evaluation of iterative transformation factor analysis. *Phys. Scrip.* **T115**, 1038–1040.

Schmeide, K., Sachs, S., Bubner, M., Reich, T., Heise, K.H., Bernhard, G., 2003. Interaction of uranium(VI) with various modified and unmodified natural and synthetic humic substances studied by EXAFS and FTIR spectroscopy. *Inorg. Chim. Acta* **351**, 133–140.

Sherman, D.M., Ragnarsdottir, K.V., Oelkers, E.H., 2000. Antimony transport in hydrothermal solutions: an EXAFS study of antimony(V) complexation in alkaline sulfide and sulfide–chloride brines at temperatures from 25 °C to 300 °C at P_{sat}. *Chem. Geol.* **167**, 161–167.

Spadini, L., Manceau, A., Schindler, P.W., Charlet, L., 1994. Structure and stability of Cd^{2+} surface complexes on ferric oxides. 1. Results from EXAFS spectroscopy. *J. Colloid Interface Sci.* **168**, 73–86.

Svensson, C., 1974. The crystal structure of orthorhombic antimony trioxide, Sb_2O_3. *Acta Crystallogr. B* **30**, 458–461.

Svensson, C., 1975. Refinement of the crystal structure of cubic antimony trioxide, Sb_2O_3. *Acta Crystallogr. B* **31**, 2016–2018.

Takaoka, M., Fukutani, S., Yamamoto, T., Horiuchi, M., Satta, N., Takeda, N., Oshita, K., Yoneda, M., Morisawa, S., Tanaka, T., 2005. Determination of chemical form of antimony in contaminated soil around a smelter using X-ray absorption fine structure. *Anal. Sci.* **21**, 769–773.

Thornton, G., 1977. A neutron diffraction study of alpha-Sb_2O_4. *Acta Crystallogr. B* **33**, 1271–1273.

Wasserman, S.R., Allen, P.G., Shuh, D.K., Bucher, J.J., Edelstein, N.M., 1999. EXAFS and principal component analysis: a new shell game. *J. Synchrotron Radiat.* **6**, 284–286.